NJC

PAPER

View Article Online
View Journal | View Issue

Cite this: *New J. Chem.*, 2019, **43**, 12340

Theoretical investigation of the chiral transition of serine and the roles of water, hydroxyl radical and hydroxide ion†

Hua Tong, ‡[a] Yan Fang Liu, ‡*[bc] Hongyan Yan, [d] Chunxu Jiang, [a] Feng Gao, [a] Zemin Mei, [e] Kun Hong, [b] Xiaocui Yang *[a] and Zuocheng Wang *[a]

We use first-principles density functional theory and *ab initio* molecular orbital theory to study the chiral transition process of the serine molecule and explore the roles of water, hydroxyl radical and hydroxide ion as catalysis during the interconversion process. The two most plausible chiral transition pathways of isolated serine are identified, in which α-hydrogen is transferred using the amino N atom as a bridge rather than the carbonyl O atom. These two chiral transition mechanisms involve the transformation of chiral enantiomers; in other words, they are serine enantiomerization. Two proton transfer steps with high energy barriers of ~58.0 and 37.0 kcal mol^{-1} are the rate-limiting steps. The calculations show that water can effectively catalyze the chiral transition by facilitating efficient proton transport, and the highest energy barriers are ~26.4 and 4.8 kcal mol^{-1}. The calculations also predict that hydroxyl radical can further lower the energy barriers of the chiral transition to approximately 12.6 and 5.3 kcal mol^{-1} by facilitating proton transfer. In contrast, hydroxyl radical is more likely to damage serine, and the damage is difficult to repair. Finally, hydroxide ion can further reduce the barriers to chiral transition to approximately 5.5 and 4.5 kcal mol^{-1} by facilitating proton transfer. As far as we know, this is the first time that these important roles of water, hydroxyl radical and hydroxide ion in serine chiral transition have been demonstrated. The findings provide new insights into the mechanism of serine enantiomerization at the atomic level. Meanwhile, the results show that hydroxyl radical can damage serine, and the damage is difficult to repair.

Received 9th April 2019,
Accepted 8th July 2019

DOI: 10.1039/c9nj01796h

rsc.li/njc

1 Introduction

Serine (Ser) is an α-amino acid containing an α-amino group, a carboxyl group, and a –CH_2OH side chain. As a chiral molecule, it has two L and D isomers (L-Ser and D-Ser) that differ in optical activity along with two *R* and *S* enantiomers (*S*-Ser and *R*-Ser) that differ in stereo-structure. The different isomers have different functions. L-Ser has many important physiological functions; it can be used to synthesize purine, thymine and choline precursors, and it is also a natural moisturizing factor that is used as an additive in cosmetics.[1] Therefore, L-Ser has a wide range of applications in medicine, food, and cosmetics.[1] D-Ser is an endogenous agonist of the *N*-methyl-D-aspartate (NMDA) receptor in the brains of mammals,[2,3] and NMDA receptors play important roles in learning, response to pain, schizophrenia, epilepsy and physiological and pathological processes. D-Ser can improve the social withdrawal of autistic patients and is clinically used to treat diseases such as schizophrenia.[4] D-Ser is also an important chiral drug intermediate with wide applications in peptide synthesis within the pharmaceutical field.[5–7] Therefore, D-Ser has strong economic potential.

L-Ser has a wide variety of sources and is low in price; in contrast, D-Ser is expensive due to its scarcity. D-Ser molecules

[a] *The Department of Physics, The Institute of Theoretical and Computational Research, Baicheng Normal University, Baicheng 137000, China. E-mail: tonghua699@126.com, yxc0622@163.com*
[b] *National & Local Joint Engineering Research Center for Mineral Salt Deep Utilization, Key Laboratory for Palygorskite Science and Applied Technology of Jiangsu Province, Huaiyin Institute of Technology, Huaian 223003, China*
[c] *Shandong Provincial Key Laboratory of Synthetic Biology, Laboratory of Biofuels, Qingdao Institute of Bioenergy and Bioprocess Technology, Chinese Academy of Sciences, Qingdao, 266061, China. E-mail: liu_yf@qibebt.ac.cn; Tel: +86-532-80662791*
[d] *Department of Computer Science, Baicheng Normal University, Baicheng 137000, China*
[e] *Department of Chemistry, Baicheng Normal University, Baicheng 137000, China*

† Electronic supplementary information (ESI) available: The corresponding energy details for all states in all pathways, and coordinates of all stationary points for all corresponding pathways. See DOI: 10.1039/c9nj01796h

‡ These authors made equal contributions to this work.

have been found in the body,[8,9] and hydroxyl radicals can cause them to be damaged. D-Ser is synthesized by the conformational transition of L-Ser in the body, termed serine chiral transition. The use of L-Ser to obtain D-Ser can generate huge economic benefits. Therefore, it is particularly important to study how L-Ser changes to D-Ser.

The chiral transition of amino acids is complicated, and the reaction mechanism is not yet fully understood. Several different mechanisms have been proposed. In 1910, Dakin[10] proposed that the optical isomerization of amino acids in solvent during the initial rate-limiting step involves the deprotonation on the alpha carbon to form a carbon anion. The protons around the amino acids then attack the alpha carbons from both directions to form L- or D-type amino acids. Based on the above mechanism, Neuberger[11] speculated that high concentrations of protons are needed for the optical isomerization of free amino acids. In this mechanism, two protons are lost from the zwitterionic amino group and methylene carbon.[12] According to Neuberger's method, Smith and Sivakua confirmed the racemization mechanism of amino acids by studying the racemic kinetics of phenylaminoacetic acid.[13] Based on quantum chemical calculations of a single gas-phase amino acid molecule, Sullivan *et al.*[14] proposed a different reaction mechanism in which alpha hydrogen transfer first transfers from the chiral carbon to the amino group, and another hydrogen atom on the amino group then transfers back to the chiral carbon atom to form the intermediate. The energy barrier for this reaction is 300 kJ mol^{-1}, which is high. Thus, it is difficult for the reaction process to be completed at low temperatures. Liardon and Schwass indicated that temperature and pH also affect the optical isomerism of amino acids.[15,16]

Previous studies have obtained the optimal geometric configurations, charge distribution, microwave spectra, LA-MB-FTMW spectra and matrix isolation infrared spectra of serine enantiomers.[17–20] At present, calculations on the racemization mechanism of serine molecules have only considered gas-phase serine molecules with intramolecular single hydrogen bonds.[21] The results show that the transfer of α-hydrogen from the α-carbon to amino nitrogen step is a rate-determining step with a total barrier of 248.0 kJ mol^{-1}. However, the exact details of the serine chiral transition mechanism from *S*-Ser to *R*-Ser have rarely been reported. The roles of water clusters, hydroxide ion water clusters and hydroxyl radical water clusters along with the solvent effects for serine chiral transition have not been reported. Previous studies also found that water molecules, hydroxyl radicals and hydroxide ions have a good catalytic effect on the proton transfer reaction in the chiral transitions α-alanine, lysine and thalidomide molecules.[22–25] The living body is a water-rich environment that contains small amounts of hydroxyl radicals and hydroxide ions, which are harmful to the organisms.[26] To understand the mechanism of serine chiral transition, in this study, several different isolated serine chiral transition mechanisms without catalysts were first considered using density functional theory (DFT) to provide a benchmark for comparison with mechanisms involving catalysts. Subsequently, several possible mechanisms of serine chiral transition catalyzed by water, hydroxyl radical and hydroxide ion were investigated. The effects of water, hydroxyl radical and hydroxide ion as catalysts on the serine chiral transition process were analysed. A better understanding of the serine chiral transition mechanism would be useful for the design of more efficient drug molecules with potential pharmaceutical and biomedical applications.

2 Computational methods and models

All geometries were optimized by DFT with the B3LYP functional and 6-31+G(d,p) basis set; more accurate energies were then obtained by performing single-point calculations at the MP2/6-311++G(2df,2pd) level.[27–37] The B3LYP functional has been used in a large number of studies on the interaction and chemical reactions in hydrogen-bonded systems, often with great success.[38–45] The solvation effects from water were considered by performing single-point calculations on the optimized structures using the SMD solvation model.[46] The analytical Hessians at the geometry optimization level of theory were carried out to obtain thermal corrections to the Gibbs free energy and the vibrational harmonic frequencies. All the stationary points as minima (zero imaginary frequency) or transition states (one imaginary frequency) were identified. There was no imaginary frequency for the minima and only one imaginary frequency for the transition state. Intrinsic reaction coordinate (IRC) analysis was performed to confirm the optimized transition state connecting the corresponding minima. Unless otherwise stated, all the final free energies presented in this study were obtained from the MP2/6-311++G(2df,2pd) level (including solvent correction) together with thermal correction to the Gibbs free energy (G_{tc}) calculated using the B3LYP/6-31+G(d,p) method. To obtain insights into the nature of the bonds between hydroxyl radicals and serine molecules, NBO analysis was performed. All calculations were performed using the Gaussian 09 program.[47]

3 Results and discussion

3.1 Properties of isolated serine

First, the chiral transition mechanism for isolated serine (*S*-Ser) was investigated. According to Fig. 1, the serine molecule consists of one hydroxyl, one amino and one carboxyl group linked by a C3–C1–C8 backbone. In the serine molecule, single intramolecular hydrogen bonds between amino and hydroxyl groups or double hydrogen bonds between amino and carboxyl groups may form. Based on a previous study of gaseous serine conformers,[20] two typical lowest-energy conformers of serine (**S_1^{A}** and **S_1^{B}**) were considered as the initial computational models (Fig. 1).

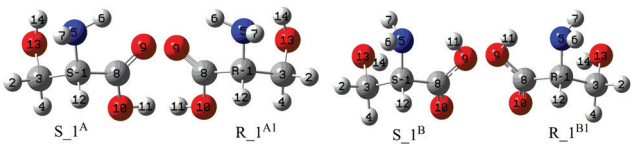

Fig. 1 Low-energy conformers from B3LYP/6-31+G(d,p) calculations and atomic labeling scheme for *S*- and *R*-type serine.

In **S_1^A**, the dihedral angles H11–O10–C8–O9, N5–C1–C8–O9, N5–C1–C3–O13, C8–C1–C3–O13 are −1.72°, 7.49°, 53.95° and −66.55°, respectively. The directions of H6 and H7 in amino N5 are swung to cover the outside. The bond lengths of C1–H12 and N5–H12 are 1.102 and 2.153 Å, respectively. Two weak hydrogen bonds are formed between the carbonyl O9 and the amino H6 (H···O = 2.233 Å), and between the amino N5 and hydroxyl H14 (H···N = 2.268 Å). Similarly, in **S_1^B**, the dihedral angles H11–O9–C8–O10, N5–C1–C8–O10, N5–C1–C3–O13, C8–C1–C3–O13 are 175.29°, −161.69°, 56.80° and −86.41°, respectively. The distances of C1–H12 and N5–H12 are 1.098 and 2.100 Å, respectively. A hydrogen bond is observed between the amino N5 and hydroxyl H14 (H···N = 1.911 Å). This reveals that the intramolecular hydrogen bonds are stronger in **S_1^B** than in **S_1^A**. The calculated results also show that **S_1^B** is more stable than **S_1^A** by about 0.55 kcal mol^{-1}. This result is in agreement with a previous study.[21]

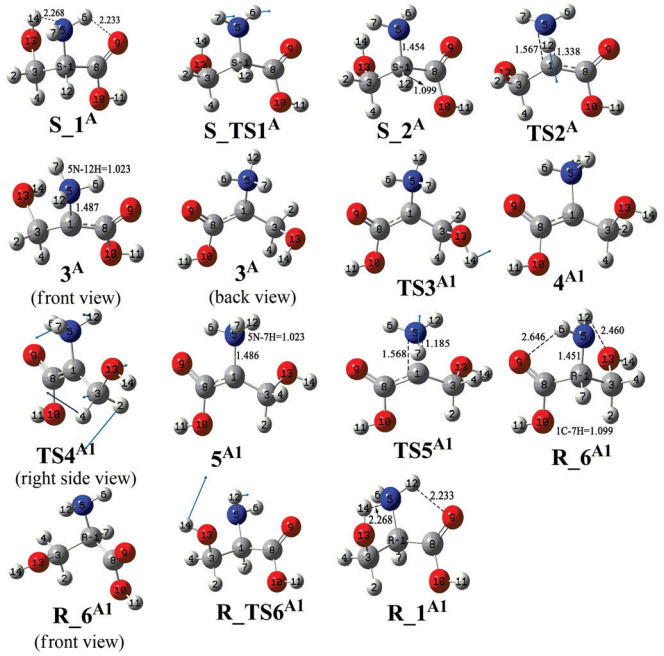

Fig. 2 Optimized structures for pathway **A1**. The arrows in the transition states show displacement vectors. Distances are given in Å.

3.2 Possible chiral transition mechanism for isolated S_1^A

To achieve the chiral transition from the *S* to *R* form of serine, the α-hydrogen needs to transfer from one side of the chiral C1 atom to the other side. For serine enantiomerization, one of a pair of enantiomers should be the mirror image of the other. Based on whether or not the interconversion is enantiomerization, two possible reaction pathways **A1** and **A2** may be responsible for the model **S_1^A**. Pathway **A1** is serine enantiomerization, and pathway **A2** is only the serine chiral transition.

Pathway **A1** (**S_1^A** enantiomerization) occurs through six steps: **S_1^A** → **S_2^A** → **3^A** → **4^{A1}** → **5^{A1}** → **R_6^{A1}** → **R_1^{A1}** (see Fig. 2). The reaction free energy profiles are shown in Fig. 3.

First, **S_1^A** isomerizes to **S_2^A** *via* transition state **S_TS1^A**. This step involves the amino isomerization, and the calculated barrier for **S_TS1^A** is 3.4 kcal mol^{-1} (see Fig. 3, Table 1 and Table S1, ESI,† which list the energies for all stationary points). During this process, the dihedral angles C6–N5–C1–C12 and C7–N5–C1–C12 rotate from +148.97° and −83.17° to +97.89° and −24.69°, respectively. Step 2 is the transfer of the H12 atom from C1 to N5 to yield **3^A** *via* the transition state **TS2^A**, during which the dihedral angle O9–C8–C1–N5 changes from −17.07° to +8.53°. Because this proton transfer is associated with bond breaking and forms highly strained three-membered rings in **3^A**, a high energy barrier must be overcome. The calculated barrier for **TS2^A** is 58.4 kcal mol^{-1} relative to **S_1^A** (Fig. 3). From **3^A**, two different pathways (pathway **A1** and **A2**) are identified according to the order of H migration and isomerization of the amino group. In pathway **A1**, step 3 involves the inverse-clockwise

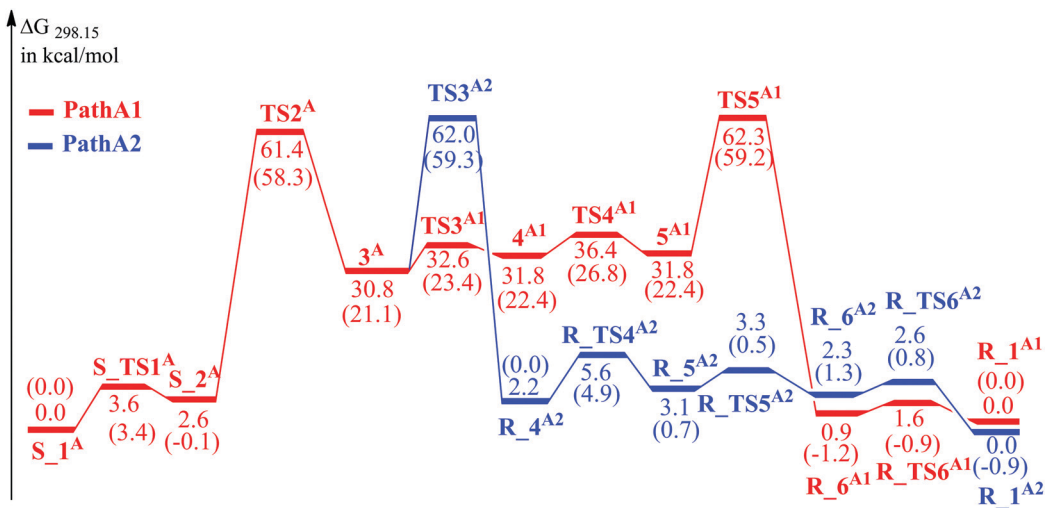

Fig. 3 Potential energy surfaces of the **S_1^A** chiral transition for pathways **A1** and **A2**. The relative free energies (*G*, in kcal mol^{-1}) are relative to structure **S_1^A**. The values in parentheses are free-energy values with solvation correction.

Table 1 Thermal correction to Gibbs free energy (G_{tc}), high-level energy (E, including the solvation correction), total energy (G_{total}), relative total energy (ΔG_{total}) and transition state imaginary frequency (Ima) at 298.15 K for all stationary points in pathway **A1**

Structures	G_{tc} (Hartree)	E (Hartree)	G_{total} (Hartree)	ΔG_{total} (kcal mol^{-1})	Ima (cm^{-1})
S_1^{A}	0.08153	−398.30825	−398.22672	0	
S_TS1^{A}	0.08001	−398.30127	−398.22126	3.43	530.32
S_2^{A}	0.08066	−398.30748	−398.22682	−0.06	
TS2^{A}	0.07552	−398.20943	−398.13391	58.29	1706.62
3^{A}	0.08121	−398.27430	−398.19309	21.12	
Pathway **A1**					
TS3^{A1}	0.08055	−398.26996	−398.18941	23.43	307.79
4^{A1}	0.08098	−398.27204	−398.19106	22.40	
TS4^{A1}	0.08042	−398.26450	−398.18408	26.78	151.89
5^{A1}	0.08098	−398.27204	−398.19106	22.40	
TS5^{A1}	0.07537	−398.20786	−398.13249	59.19	1703.54
R_6^{A1}	0.08059	−398.30924	−398.22865	−1.21	
R_TS6^{A1}	0.08039	−398.30856	−398.22817	−0.91	230.00
R_1^{A1}	0.08153	−398.30825	−398.22672	0.00	
Pathway **A2**					
TS3^{A2}	0.07528	−398.20760	−398.13232	59.29	1703.50
R_4^{A2}	0.08067	−398.30750	−398.22683	−0.04	
R_TS4^{A2}	0.07933	−398.29827	−398.21894	4.89	589.15
R_5^{A2}	0.08036	−398.30600	−398.22564	0.68	
R_TS5^{A2}	0.08016	−398.30476	−398.2246	1.33	237.77
R_6^{A2}	0.08036	−398.30578	−398.22542	0.82	
R_TS6^{A2}	0.08040	−398.30523	−398.22483	1.19	218.04
R_1^{A2}	0.08128	−398.30948	−398.2282	−0.93	

rotation of the hydroxyl –O13H14 along the C3–O13 axis; that is, **3^{A}** (H4–C3–O13–H14 = −53.35°) isomerizes to **4^{A1}** (H4–C3–O13–H14 = 69.73°) *via* a transition state **TS3^{A1}** (H4–C3–O13–H14 = 16.35°). This hydroxyl group rotation must overcome an energy barrier of only 2.3 kcal mol^{-1}. This step is accompanied by changes in the dihedral angles C1–C3–O13–H14 and N5–C1–C3–O13 from 69.65° and 55.03° to −171.17° and 48.67°, respectively. Step 4 involves the inverse-clockwise rotation of dihedral angles H4–C3–O13–H14 along the C1–C3 axis; that is, **4^{A1}** (5N–1C–3C–H4 = 169.19°) isomerizes to the corresponding stereotactic enantiomer **5^{A1}** (5N–1C–3C–H4 = 70.25°) *via* a transition state **TS4^{A1}** (5N–1C–3C–H4 = 119.58°), overcoming a barrier of 2.4 kcal mol^{-1} (see Table 1). In step 5, the *S*-type **5^{A1}** changes to *R*-type **R_6^{A1}** *via* transition state **TS5^{A1}**, overcoming an energy barrier of 36.8 kcal mol^{-1}. The transfer of H7 atom from N5 to C1 occurs in this step, accompanied by a change in the dihedral angle C12–N5–C6–C7 from −120.25° to 146.65°, and the C1–C7 bond length changes from 2.13 to 1.10 Å. In this step, the proton transfers from one side of chiral C1 to the other side, and the chiral conversion of **S_1^{A}** is completed.

Finally, similar to the amino isomerization in the first step, **R_6^{A1}** changes to the corresponding enantiomer **R_1^{A1}** *via* a transition state **R_TS6^{A1}** (0.3 kcal mol^{-1}) to achieve the chiral enantiomer conversion of **S_1^{A}**. During this step, the orientation of two H6 and H12 atoms in amino N5 is swung to cover the inside from outside; meanwhile, the dihedral angle C1–C3–O13–H14 rotates along the C1–C3 axis, the C8–C1–N5–H12 angle rotates along the C8–C1 axis, and the dihedral angles C1–C3–O13–H14 and C8–C1–N5–H12 change from 173.83° and −68.65° to 46.03° and 19.69°, respectively. The results show that **R_1^{A1}** and **S_1^{A}** are stereoisomers that are non-superimposable mirror images of each other. In other words, their bond lengths and angles are exactly the same, the absolute values of their dihedral angles are the same, and their directions are opposite (the details are shown in Table S2, ESI†). Therefore, **S_1^{A}** achieves the chiral enantiomer transition *via* pathway **A1**.

In pathway **A2**, the chiral transition of **S_1^{A}** also involves six steps: **S_1^{A}** → **S_2^{A}** → **3^{A}** → **R_4^{A2}** → **R_5^{A2}** → **R_6^{A2}** → **R_1^{A2}** (see Fig. 4). In this pathway, the proton transfer occurs first followed by the isomerization of the hydroxyl and amino groups.

First, H7 atom transfers from N5 to C1; that is, **3^{A}** isomerizes to **R_4^{A2}** *via* a transition state **TS3^{A2}**. This process is similar to the fifth step of pathway **A1** and needs to overcome an energy barrier of 38.2 kcal mol^{-1}. Next is the isomerization of the amino; that is, **R_4^{A2}** changes to **R_5^{A2}** *via* a transition state **R_TS4^{A2}**, which is accompanied by changes in the positions of

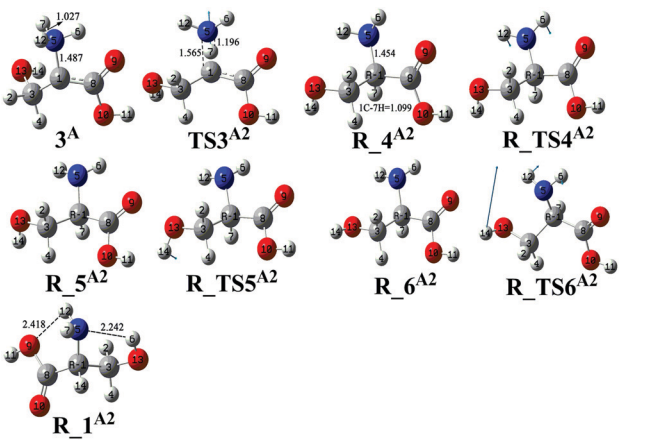

Fig. 4 Optimized structures for pathway **A2**. The arrows in the transition states show displacement vectors. Distances are given in Å.

both H6 and H12 from outside to inside the cover, whereas the dihedral angle H7–C1–N5–H12 changes from 83.82° to 56.83°. The barrier of this step is predicted to be only 4.9 kcal mol^{-1}. Subsequently, **R_5^{A2}** isomerizes to **R_6^{A2}** *via* a transition state **R_TS5^{A2}**, overcoming a barrier of only 0.2 kcal mol^{-1}. When the solvation correction is considered, it becomes a barrierless process (see Table 1 and Table S1, ESI†). From **R_5^{A2}** to **R_6^{A2}**, the dihedral angle C1–C3–O13–H14 rotates along the C3–O13 axis and changes from 82.27° to −167.77°. Finally, **R_6^{A2}** isomerizes the **R_1^{A2}** *via* a transition state **R_TS6^{A2}** to complete the chiral conversion of **S_1^{A}** (0.4 kcal mol^{-1} without the solvation correction and −0.5 kcal mol^{-1} with the solvation correction). This last step is the same as that in pathway **A1**. In this step, the dihedral angle C1–C3–O13–H14 rotates along the C1–C3 axis in concert with the rotation of the C7–C1–N5–H12 angle along the C7–C1 axis, whereas the dihedral angles C1–C3–O13–H14 and C7–C1–N5–H12 change from −167.77° and −70.24° to −44.23° and −157.27°, respectively. In **R_1^{A2}**, the distances of N5–H14, O9–H12 and O10–H4 are 2.24, 2.47 and 2.77 Å, respectively.

As discussed above, the first proton transfer step (N5 → C1) is the second step and a rate-determining step with a total barrier of 58.4 kcal mol^{-1}. After the first proton transfer, the barriers of the rate-determining step (proton transfer from C1 to N5) for pathways **A1** and **A2** are 36.8 and 38.2 kcal mol^{-1}, respectively, which can be considered equal within the range of error. This indicates that the chiral transformation of isolated **S_1^{A}** is equally likely to occur through pathways **A1** and **A2**. However, the transformation of enantiomers only occurs *via* pathway **A1**. As far as we know, the "limit energy barrier" of the proton migration is 39.95 kcal mol^{-1}; however, 58.4 kcal mol^{-1} is higher than 39.95 kcal mol^{-1},[48,49] indicates that it is difficult to complete the chiral transition of isolated **S_1^{A}** without catalysts.

3.3 Possible chiral transition mechanism for isolated S_1^{B}

Three possible reaction pathways, **B1**, **B2** and **B3**, are proposed based on whether or not they can complete the chiral enantiomer transformation of **S_1^{B}**.

Pathway **B1**: the chiral enantiomer transition of **S_1^{B}** occurs through eight steps: **S_1^{B}** → **S_2^{B}** → **3^{B}** → **4^{B1}** → **5^{B1}** → **R_6^{B1}** → **R_7^{B1}** → **R_8^{B1}** → **R_1^{B1}** (see Fig. 5).

Step 1 involves rotation of the dihedral angles C1–C8–O9–H11 along the C1–C8 axis; that is, **S_1^{B}** (C1–C8–O9–H11 = −5.50°) isomerizes to **S_2^{B}** (C1–C8–O9–H11 = 178.22°) *via* a transition state **S_TS1^{B}** (C1–C8–O9–H11 = 93.64°; see Fig. 5). The rotation needs to overcome an energy barrier of 13.1 kcal mol^{-1} (Fig. 6, Table 2 and Table S3, ESI,† which list the energies for all stationary points). During this step, the dihedral angle H11–O9–C8–O10 also changes from 175.29° to −3.06°, whereas the angle H6–N5–C1–H12 changes from −33.77° to −52.13°. In step 2, **S_2^{B}** changes to **3^{B}** *via* a transition state **TS2^{B}**, in which the H12 atom transfers from C1 to N5. As a result, the amino protonated. This process is similar to the second step of pathway **A1**. In this step, the dihedral angle C3–C1–N5–H6 changes from 79.18° to −39.75°, and the bond length of C1–H12 changes from 1.09 to 1.35 Å. This step is similar to the second step of pathway **A1** and is associated with bond breaking; thus, a high energy barrier of

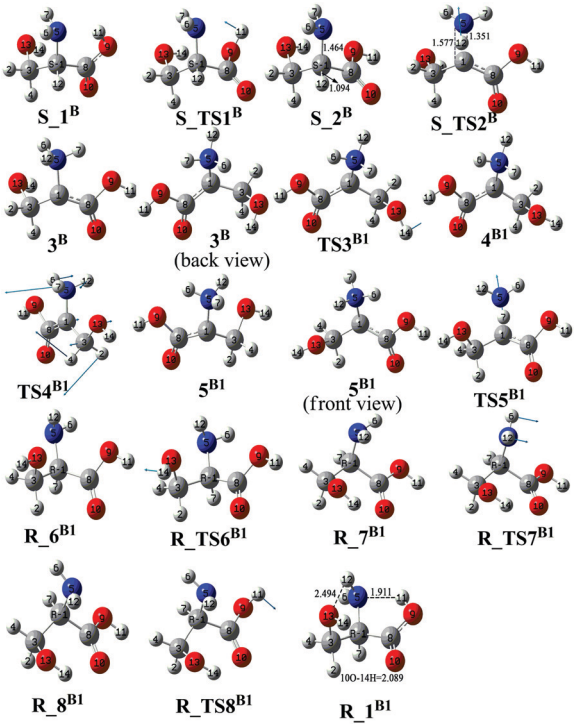

Fig. 5 Optimized structures for pathway **B1**. The arrows in the transition states show displacement vectors. Distances are given in Å.

~57.7 kcal mol^{-1} must be overcome (Fig. 6 and Table 2 and Table S3, ESI†). Step 3 involves the rotation of the dihedral angle C1–C3–O13–H14 along the C1–C3 axis; that is, **3^{B}** (C1–C3–O13–H14 = 74.05°) isomerizes to **4^{B1}** (C1–C3–O13–H14 = 178.22°) *via* a transition state **TS3^{B1}** (C1–C3–O13–H14 = −171.96°; see Fig. 5). The barrier of this rotation was calculated to be 2.0 kcal mol^{-1}. In step 4, **4^{B1}** isomerizes to **5^{B1}** *via* the transition state **TS4^{B1}**, overcoming a barrier of 2.4 kcal mol^{-1} (see Fig. 6). This step involves the rotation of the dihedral angle C8–C1–C3–H4 along the C1–C3 axis in concert with the rotation of the angle C8–C1–N5–H7 along the C8–C1 axis, whereas the dihedral angles C8–C1–C3–H4 and C8–C1–N5–H7 change from 18.31° and 113.12° to −139.44° and 125.75°, respectively. In step 5, the H7 atom transfers from N5 to C1 to yield *R*-type **R_6^{B1}** *via* a transition state **TS5^{B1}**, accompanied by a change in the dihedral angle H6–N5–C1–H7 from −108.77 to −67.18° and a decrease in the C1–H7 bond length from 2.13 to 1.10 Å. Finally, the hydrogen atom transfers from one side of C1 to the other side to complete the chiral conversion of **S_1^{B}**. This process needs to overcome an energy barrier of 36.9 kcal mol^{-1}. Step 6 is the similar to step 3 and also involves the rotation of the dihedral angle C1–C3–O13–H14 along the C1–C3 axis; that is, **R_6^{B1}** (C1–C3–O13–H14 = 179.72°) isomerizes to **R_7^{B1}** (C1–C3–O13–H14 = −67.76) *via* the transition state **R_TS6^{B1}** (C1–C3–O13–H14 = −136.48°; see Fig. 5). The energy barrier of this rotation was calculated to be 0.6 kcal mol^{-1} relative to **S_1^{B}**. Step 7 involves the isomerization of the amino; that is, **R_7^{B1}** isomerizes to **R_8^{B1}** *via* transition state **R_TS7^{B1}**, for which the energy was calculated to be only 4.9 kcal mol^{-1}

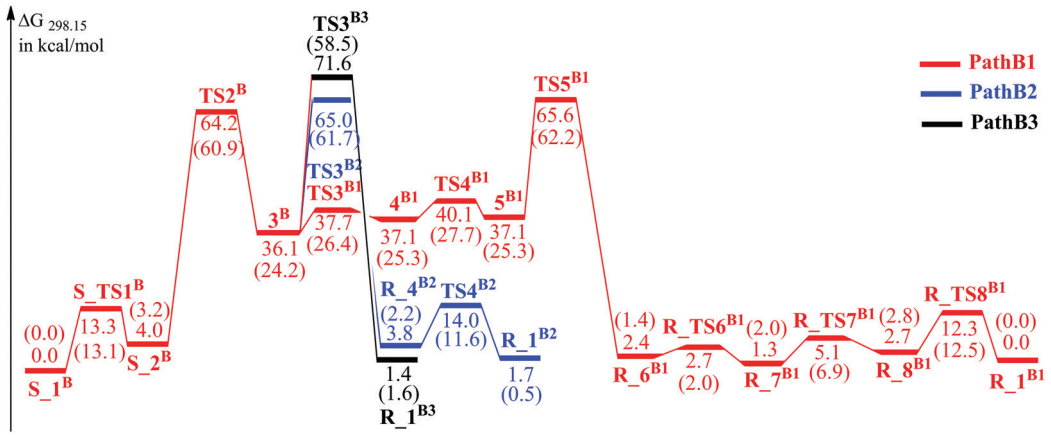

Fig. 6 Potential energy surfaces of the **S_1^{B}** chiral transition for pathways **B1**, **B2** and **B3**. The relative free energies (G, in kcal mol^{-1}) are relative to structure **S_1^{B}**. The relative free energies with solvation correction are shown in parentheses.

Table 2 High-level energy (E, including the solvent correction), thermal correction to the Gibbs free energy (G_{tc}), total energy (G_{total}, including the ZPE correction), relative total energy (ΔG_{total}) and transition state imaginary frequency (Ima) at 298.15 K for all stationary points in each reaction channel of the **S_1^{B}** chiral transition to **R_1^{B}**

Structures	G_{tc} (Hartree)	E (Hartree)	G_{total} (Hartree)	ΔG_{total} (kcal mol^{-1})	Ima (cm^{-1})
S_1^{B}	0.08194	−398.31126	−398.22932	0.00	
S_TS1^{B}	0.07982	−398.28816	−398.20834	13.18	539.83
S_2^{B}	0.08104	−398.30520	−398.22416	3.24	
TS2^{B}	0.07517	−398.20749	−398.13232	60.93	1685.36
3^{B}	0.08104	−398.27183	−398.19079	24.20	
Pathway **B1**					
TS3^{B1}	0.08035	−398.26768	−398.18733	26.37	282.33
4^{B1}	0.08069	−398.26966	−398.18897	25.34	
TS4^{B1}	0.07794	−398.26324	−398.1853	27.65	163.34
5^{B1}	0.08069	−398.26966	−398.18897	25.34	
TS5^{B1}	0.07515	−398.20552	−398.13037	62.15	1685.20
R_6^{B1}	0.08055	−398.30765	−398.2271	1.39	
R_TS6^{B1}	0.08041	−398.30652	−398.22611	2.01	201.95
R_7^{B1}	0.08154	−398.30764	−398.2261	2.02	
R_TS7^{B1}	0.08028	−398.29855	−398.21827	6.94	581.04
R_8^{B1}	0.08156	−398.30637	−398.22481	2.83	
R_TS8^{B1}	0.08017	−398.28967	−398.2095	12.45	605.12
R_1^{B1}	0.08194	−398.31126	−398.22932	0.00	
Pathway **B2**					
TS3^{B2}	0.07496	−398.20599	−398.13103	61.73	1684.38
R_4^{B2}	0.08035	−398.30619	−398.22584	2.19	
R_TS4^{B2}	0.07885	−398.28962	−398.21077	11.65	576.12
R_1^{B2}	0.08189	−398.31040	−398.22851	0.51	
Pathway **B3**					
TS3^{B3}	0.07733	−398.21359	−398.13626	58.45	1657.50
R_1^{B3}	0.08088	−398.30765	−398.22677	1.60	

relative to complex **1**. During this step, two H6 and H12 atoms change to the opposite direction, whereas the dihedral angle C6–N5–C1–H7 changes from −66.67° to 39.90° (Fig. 6). Finally, **R_8^{B1}** isomerizes to easily isomerize the corresponding enantiomer **R_1^{B1}** *via* transition state **R_TS8^{B1}** to complete the chiral enantiomer conversion of **S_1^{B}** (9.7 kcal mol^{-1}). In this step, the dihedral angle C1–C8–O9–H11 rotates along the C1–C8 axis, whereas the dihedral angle C1–C8–O9–H11 changes from 176.35° to 5.49°. In **R_1^{B1}**, the bond lengths of N5–H11, O13–H12 and O10–H14 are 1.91, 2.49 and 2.81 Å, respectively.

From **3^{B}**, two different chiral transition pathways (pathways **B2** and **B3**) have been identified according to the different pathways of H migration.

Pathway **B2**: the chiral transition of **S_1^{B}** occurs through four steps, **S_1^{B}** → **S_2^{B}** → **3^{B}** → **R_4^{B2}** → **R_1^{B2}** (see Fig. 7).

In pathway **B2**, the third step involves the transfer of the H6 atom from N5 to C1; that is, **3^{B}** isomerizes to **R_4^{B2}** *via* **TS3^{B2}**. In this process, the proton is transferred from one side of C1 to the other side, completing the chiral conversion of **S_1^{B}**. This proton transfer needs to overcome an energy barrier of

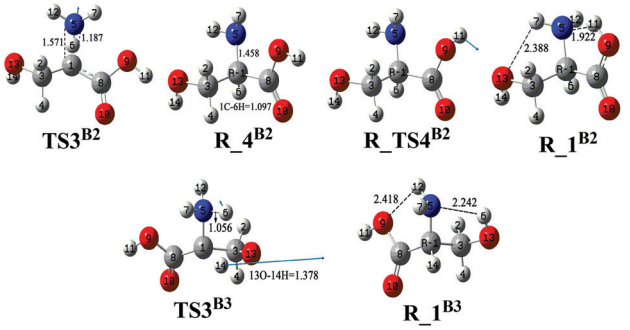

Fig. 7 Optimized structures for pathway **B2**. The arrows in the transition states indicate the vibrational direction of the imaginary frequency. Distances are given in Å.

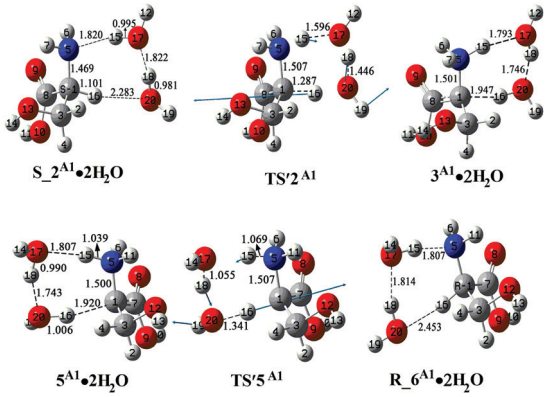

Fig. 8 Optimized geometries for water dimer-mediated proton transfer reactions (**S_2^{A1}·2H$_2$O** → **3^{A1}·2H$_2$O** and **5^{A1}·2H$_2$O** → **R_6^{A1}·2H$_2$O**). The arrows in **TS′2^{A1}** and **TS′5^{A1}** show displacement vectors. Distances are given in Å.

37.5 kcal mol^{-1}. This step is accompanied by a change in the dihedral angle H12–N5–C1–H6 from 120.89° to 72.37° and a change in the bond length 5N–6H from 1.03 to 2.08 Å. Finally, the dihedral angle C1–C8–O9–H11 rotates along the C1–C8 axis, producing the corresponding enantiomer **R_1^{B2}** *via* the transition state **TS4^{B2}** to complete the chiral conversion of **S_1^{B}**. The barrier of this step is predicted to be 9.4 kcal mol^{-1}. In this step, the dihedral angle C1–C8–O9–H11 changes from 178.15° to −2.63°.

In the alternative pathway **B3**, **3^{B}** is converted to product **R_1^{B3}** *via* the transition state **TS3^{B3}** to complete the chiral transition of **S_1^{B}** (see Fig. 7), overcoming a barrier of 34.3 kcal mol^{-1} (see Fig. 6 and Table 2). During this step, H14 atom transfers from the hydroxyl O13 to the chiral carbon C1 in concert with the transfer of H6 from amino N5 to hydroxyl O13. As a result, the bond distance of 5N–6H elongates from 0.97 to 1.38 Å. Meanwhile, the dihedral angle 5N–1C–8C–3C changes from −146.65° to 136.30°.

As discussed above, the second elemental reaction is a rate-determining step for the chiral transition of **S_1^{B}**, with a total barrier of 57.7 kcal mol^{-1}. The calculated rate-determining energy barriers for the above four pathways (**A1**, **A2**, **B1** and **B2**) are similar (~60.0 kcal mol^{-1}). The high barriers for these four pathways indicate that no reaction can occur under isolated conditions. To complete the **S_1^{A}** and **S_1^{B}** chiral transitions, the catalyst has to lower the barrier by at least 30 kcal mol^{-1}.

3.4 Water-, hydroxyl radical- and hydroxide ion-catalysed proton transfer (S_2^{A} → 3^{A1} and 5^{A1} → R_6^{A1})

For isolated *S*-Ser enantiomerization, there are two high-energy barriers (≈58 and 37 kcal mol^{-1}) for the proton transfer steps (**TS2^{A1}** and **TS5^{A1}**) in the most favorable pathway, indicating that no reaction can occur under isolated conditions. First, inspired by previous reports,[24,50,51] we introduced a water dimer in the two proton transfer steps as a bridge to facilitate proton transfer *via* the Grotthuss mechanism.[24,52] In other words, a water dimer is placed between the H16 and N5 atoms in **S_2^{A1}**, and a water dimer is positioned between the H15 and C1 atoms in **5^{A1}**. The optimized geometries of each state for the **S_2^{A1}·2H$_2$O** → **3^{A1}·2H$_2$O** and **5^{A1}·2H$_2$O** → **R_6^{A1}·2H$_2$O** steps are presented in Fig. 8 and Table S4 (ESI†). The **S_2^{A1}·2H$_2$O** complex shows three hydrogen bonds between H16 of **S_2^{A}** and O20 of the water dimer, between N5 of **S_2^{A}** and H15 of the water dimer, and between H18 and O17 of the water dimer, with bond distances of 2.28, 1.82 and 1.82 Å, respectively. Starting from **S_2^{A1}·2H$_2$O**, H16 departs from C1 and moves towards O20, H18 departs from O20 and moves towards O17, and H15 departs from O17 and moves towards N5. As a result, a proton hops to N5 from the original C1 atom *via* the "water bridge," creating the intermediate **3^{A1}·2H$_2$O** (see Fig. 8). Here, the role of the water molecule is similar to that in the enantiomerization of thalidomide.[24] These findings are further confirmed by IRC calculations. The associated energy barrier was calculated to be 26.4 kcal mol^{-1} relative to **S_2^{A1}·2H$_2$O**, which is much lower than that for isolated *S*-Ser (58.4 kcal mol^{-1}). From **TS′2^{A1}** to **3^{A1}·2H$_2$O**, the key distances of H6–C1, O20–H18 and O7–H5 are elongated from 1.29, 1.45 and 1.60 Å to 1.95, 1.75 and 1.79 Å, respectively.

Similarly, H15 departs from N5 and moves towards O17, H18 departs from O17 and moves towards O20, and H16 departs from O20 and moves toward C1 for the **5^{A1}·2H$_2$O** → **R_6^{A1}·2H$_2$O** step (see Fig. 8). As a result, a proton hops from the original position of the N5 atom to the C1 atom *via* water functioning as a bridge. The IRC calculations further confirm this mechanism. The energy barrier of these proton transfers for **TS′5^{A1}** is 5.6 kcal mol^{-1} (see Fig. 9), which is much lower than that for isolated *S*-Ser (36.8 kcal mol^{-1}).

A large number of hydroxyl radicals are generated in the living body as the organism ages. To understand hydroxyl radical-catalysed serine enantiomerization, we inserted an aqueous cluster of hydroxyl radical, **H$_2$O·OH$^{\bullet}$**, into the proton transfer step of **S_1^{A}** enantiomerization. The **H$_2$O·OH$^{\bullet}$**-catalysed serine enantiomers are shown in Fig. 10. In **S_2^{A1}·(H$_2$O·OH$^{\bullet}$)**, the hydrogen bond (H14···N5 = 1.76 Å) formed by N5 of **S_2^{A1}** and H14 of the hydroxyl radical is stronger than that (H15···N5 = 1.82 Å) formed by N5 of **S_2^{A1}** and H15 of water because the hydroxyl radical has stronger electronegativity than water. However, the hydrogen bonds (H15···O19 = 2.35 Å and H17···O16 = 1.89 Å) formed by H15 of **S_2^{A1}** and O19 of water

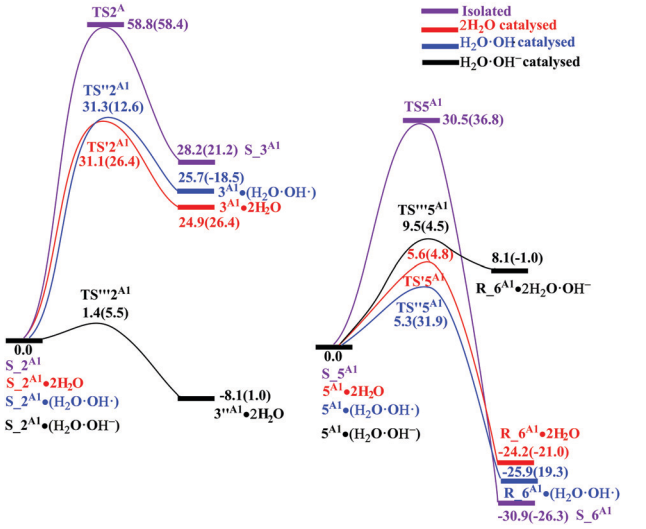

Fig. 9 Energies for the water dimer-, hydroxyl radical- and hydroxide ion-catalysed proton transfer reactions calculated at the MP2/6-311++G(2df,2pd) level of theory. The relative free energies (G, in kcal mol^{-1}) with solvation correction are shown in parentheses.

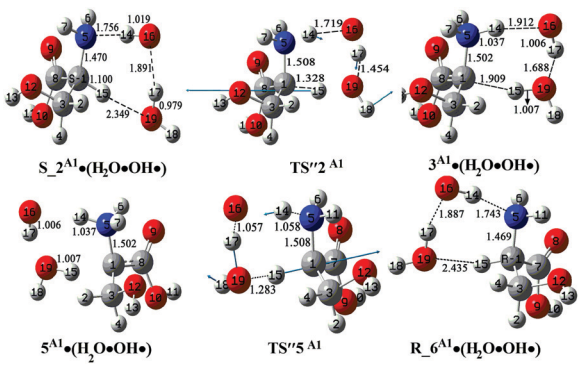

Fig. 10 Optimized geometries for the hydroxyl radical-mediated proton transfer reactions of **S_2^{A1}·(H$_2$O·OH•)** → **3^{A1}·(H$_2$O·OH•)** and **5^{A1}·(H$_2$O·OH•)** → **R_6^{A1}·(H$_2$O·OH•)**. The arrows in **TS''2^{A1}** and **TS''5^{A1}** show displacement vectors. Distances are given in Å.

and by O17 of water and O16 of hydroxyl radical are weaker than those (H16···O20 = 2.28 Å and H19···O17 = 1.82 Å) formed by H16 of **S_2^{A1}** and O20 of water and by H19 and O17 of water dimer. In **TS''2^{A1}**, H14 transfers from O16 to N5, H17 transfers from O19 to O16, and H15 transfers from C1 to O19, implying that a proton jumps from the original position of the C1 atom to the N5 atom across the "**H$_2$O·OH•** bridge." The associated energy barrier is 12.6 kcal mol^{-1} relative to **S_2^{A1}·(H$_2$O·OH•)**, which is 46 kcal mol^{-1} lower than that for isolated *S*-Ser (see Fig. 9 and Table S5, ESI†). These findings can be further confirmed by IRC calculations (see Fig. S1 and S2, ESI†). The formed intermediate **3^{A1}·(H$_2$O·OH•)** shows poor stability with an energy of 25.7 kcal mol^{-1} (−18.5 kcal mol^{-1} considering the solvation effect) relative to complex **S_2^{A1}·(H$_2$O·OH•)** (Fig. 9). The details are shown in the ESI† (Fig. S3).

For the **H$_2$O·OH•**-catalyzed proton transfer step of **5^{A1}** → **R_6^{A1}**, we also optimized the transition state **TS''5^{A1}** (Fig. 10), which corresponds to proton transfer across the "(**H$_2$O·OH•**) bridge," in which H14 moves away from N5 and toward O16, H17 moves away from O16 and toward O19, and H15 moves away from O19 and toward C1. The O16 atom can tightly hold a proton; thus, the associated energy barrier is 31.9 kcal mol^{-1} (5.3 kcal mol^{-1} without the solvation correction) relative to **5^{A1}·(H$_2$O·OH•)**, lower than that for isolated *S*-Ser (see Fig. 9 and Table S5, ESI†).

Finally, we put an aqueous cluster of hydroxide ion (**H$_2$O·OH$^-$**) [a simplified form of the OH$^-$·(H$_2$O)$_n$ cluster that exists in basic solution][24] into the proton transfer step of the **S_1^{A}** chiral transition process to understand base-catalysed enantiomerization. The optimized structures for OH$^-$·H$_2$O-mediated chiral transition are shown in Fig. 11. Unlike in the above reactants, in **S_2^{A1}·(H$_2$O·OH$^-$)**, the O19 atom of OH$^-$ and the O16 atom of water are connected with the H15 and H6 atoms of **S_2^{A}** by hydrogen bonds with distances of 1.79 and 2.19 Å. From the transition state **TS'''2^{A1}**, H15 transfers from C1 to O19, and the OH$^-$·H$_2$O cluster becomes a water dimer. The calculated barrier for **TS'''2^{A1}** is 5.5 kcal mol^{-1} relative to **S_2^{A1}·(H$_2$O·OH$^-$)**, which is 53 kcal mol^{-1} lower than that for isolated *S*-Ser (see Fig. 9 and Table S6, ESI†).

After the process of proton transfer (**S_2^{A1}·(H$_2$O·OH$^-$)** → **3''^{A1}·2H$_2$O**), it is reasonable to propose the following two possibilities based on a previous study.[29] (1) The negatively charged molecule **3''^{A1}** seizes a proton from the surrounding solution to form **3^{A}**, the proton of serine undergoes a series of conformational changes (similar to steps 3 and 4 of pathway **A1** for isolated serine and step 5 for water-assisted proton transfer, see Fig. 2 and 11), thus completing the serine enantiomerization. The highest calculated activation energy in all of the above processes is expected to be ∼5.5 kcal mol^{-1}. (2) The proton-less serine undergoes a series of conformational changes to form **5'^{A1}** (here, **5'^{A1}** refers to **R_6^{A1}** after the loss of H15, see Fig. 2). The central C1 atom then seizes a proton from the surrounding water molecule to form **R_6^{A1}·(H$_2$O·OH$^-$)** from **5'^{A1}·2H$_2$O**. Finally, **R_6^{A1}** undergoes a series of conformational changes to accomplish the enantiomerization process. The highest

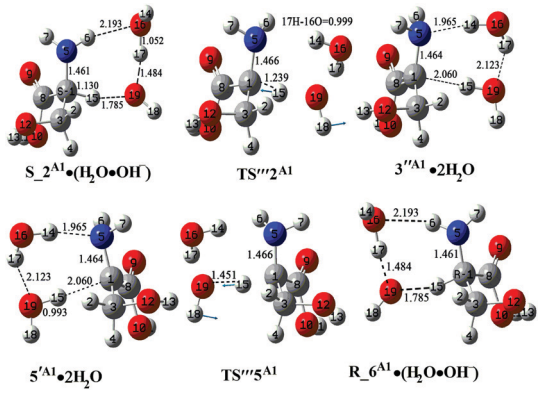

Fig. 11 Optimized geometries for the hydroxide ion-mediated proton transfer reactions of **S_2^{A1}·(H$_2$O·OH$^-$)** → **3''^{A1}·2H$_2$O** and **5'^{A1}·2H$_2$O** → **R_6^{A1}·(H$_2$O·OH$^-$)**. The arrows in **TS'''2^{A1}** and **TS'''5^{A1}** show displacement vectors. Distances are given in Å.

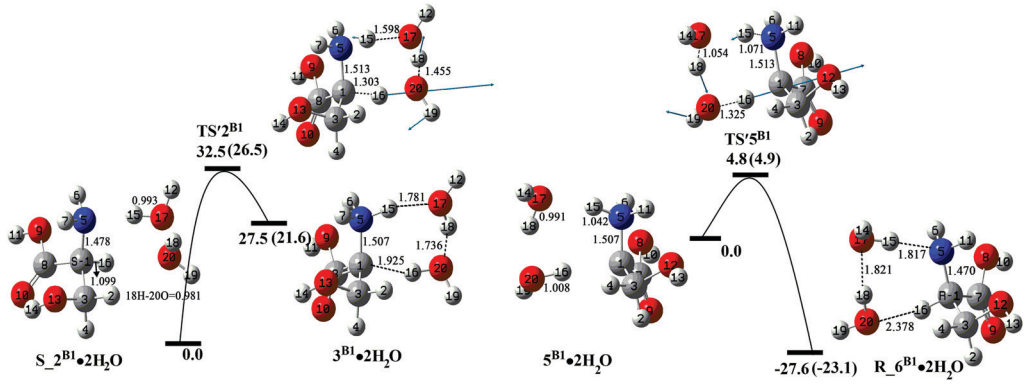

Fig. 12 Optimized geometries and corresponding energies (in kcal mol^{-1}) of the water dimer-mediated proton transfer reactions (**S_2^{B1}·2H$_2$O** → **3^{B1}·2H$_2$O** and **5^{B1}·2H$_2$O** → **R_6^{B1}·2H$_2$O**) calculated at the MP2/6-311++G(2df,2pd) level of theory. The values in parentheses include the solvation correction. The arrows in **TS′2^{B1}** and **TS′5^{B1}** show displacement vectors. Distances are given in Å. Energies are shown in kcal mol^{-1}.

energy barrier in all of the above processes is approximately 4.5 kcal mol^{-1}.

3.5 Water-catalysed proton transfer (S_2^{B1} → 3^{B1} and 5^{B1} → R_6^{B1})

Similarly, for pathway **B1**, we also introduced two water molecules to facilitate proton transfer in the **S_2^{B1}·2H$_2$O** → **3^{B1}·2H$_2$O** and **5^{B1}·2H$_2$O** → **R_6^{B1}·2H$_2$O** steps. The optimized structures of the reaction and the corresponding free energies are shown in Fig. 12 and Table S7 (ESI†). During this process, proton transfer occurs from the original position of the N5 atom to the C1 atom (C1 → N5) through the "water bridge."[24] As a consequence, the energy barriers of these proton transfers (**TS′2^{B1}** and **TS′5^{B1}**) are 26.5 and 4.9 kcal mol^{-1} compared to 58.4 and 36.8 kcal mol^{-1} for isolated *S*-Ser, respectively (see Fig. 6 and 12).

3.6 Hydroxyl radical-catalysed serine damage

We changed the position of OH$^{\bullet}$ and H$_2$O, meaning that we introduced [(OH$^{\bullet}$)·H$_2$O)] instead of (**H$_2$O·OH$^{\bullet}$**) into the proton-abstraction step of **S_1^{A}** enantiomerization. The optimized structures of the reactant, transition state (**TS′′′′2^{A1}**) and product and corresponding free energy profiles for this reaction are shown in Fig. 13 (for details, see Table S8, ESI†). In **S_2^{A1}·[(OH$^{\bullet}$)·(H$_2$O)]**, the H15 atom of water and N5 atom of **S_2^{A}** are connected by hydrogen bonds (H15···N5 = 1.80 Å), and the O19 atom of (OH$^{\bullet}$) and H16 atom of **S_2^{A}** are connected by hydrogen bonds (H16···O19 = 2.53 Å). The obtained transition state **TS′′′2^{A1}** corresponds to the proton transfer across the "**[(OH$^{\bullet}$)·(H$_2$O)]** bridge," in which H16 transfers from C1 to O19.[24] After H16 transfers from C1 to O19, the cluster **[(OH$^{\bullet}$)·(H$_2$O)]** becomes a water dimer, which shares hydrogen bonds (N5···H15 = 2.03 Å and H2···O19 = 2.31 Å) with **3′^{A1}** (here, **3′^{A1}** is formed by the loss of H16 from **S_2^{A1}**). As a consequence, the C1 atom of product **3′^{A1}** loses its chirality, and **3′^{A1}** loses the serine functionality. These findings can be further confirmed by IRC calculations (see Fig. S4 and S5, ESI†). The activation energy is computed to be 7.0 kcal mol^{-1} in this process; as a result, the formation of a stable product **3′^{A1}·2(H$_2$O)** is exothermic by 39.5 kcal mol^{-1} relative to complex **S_2^{A1}·[(OH$^{\bullet}$)·H$_2$O)]** (Fig. 13), indicating that hydroxyl radical can cause serine damage, which is difficult to repair. Details are shown in the ESI† (Fig. S6).

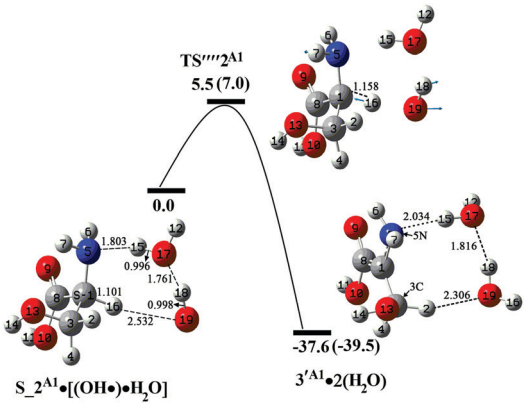

Fig. 13 Optimized structures and corresponding energies (in kcal mol^{-1}) for the hydroxyl radical-mediated proton transfer reactions of **S_2^{A1}·[(OH$^{\bullet}$)·H$_2$O)]** → **3′^{A1}·2(H$_2$O)** calculated at the MP2/6-311++G(2df,2pd) level of theory. The values in parentheses are calculated free-energy values in the solvent phase. The arrows in **TS′′′′2^{A1}** show displacement vectors. Distances are given in Å.

4 Conclusions

In the present study, DFT calculations were used to study the chiral transition mechanism of serine and the roles of water molecules, hydroxyl radicals and hydroxide ion in the interconversion process. For isolated serine, two typical lowest-energy conformers of serine (**S_1^{A}** and **S_1^{B}**)[14] were taken as computational models based on previous experimental and computational observations[20,21] as well as the formation of different types of hydrogen bonds. Based on the calculations, we proposed two preferred reaction mechanisms (**A1** and **B1**) in which α hydrogen transfers to amino N from chiral C1 and then to another side of chiral C1 using amino N as a bridge. In other words, α hydrogen transfers only by using amino N as a bridge

without using carbonyl O, consistent with previous studies.[21] It is worth noting that both mechanisms are serine enantiomerization. However, for both mechanisms, the reaction does not occur spontaneously under isolated conditions since they have remarkably high energy barriers of $\sim$58.0 and 37.0 kcal mol^{-1} for the proton transfer steps. The high barriers indicate that the reactions do not take place under isolated conditions.

The catalytic reactions in which water molecules, hydroxyl radicals and hydroxide ions act as catalysts were considered. First, water molecules were demonstrated to be a good catalyst to facilitate proton transfer in the chiral transition using the Grotthuss mechanism; water molecules were found to dramatically reduce the highest energy barrier of chiral conversion to 30 kcal mol^{-1}. Second, hydroxyl radical was shown to effectively catalyze serine enantiomerization by assisting proton transfer; hydroxyl radical was found to reduce the highest energy barriers of chiral conversion to approximately 12.6 and 5.3 kcal mol^{-1}. Meanwhile, hydroxyl radical was found to cause serine damage, which is difficult to repair, with the activation energy of 7.0 kcal mol^{-1}. Finally, hydroxide ion was demonstrated to catalyze the chiral conversion of serine with high catalytic efficiency; hydroxide ion was found to reduce the barrier to chiral transition to approximately 5.5 and 4.5 kcal mol^{-1} by facilitating proton transfer.

Conflicts of interest

There are no conflicts to declare.

Acknowledgements

This work is supported by the National Natural Science Foundation of China (Grant No. 21607164) and Grants from Jilin Province Science and Technology Development Project in China (No. 20130101131JC). The authors also thank Professor Zhigang Wang (Jilin University) and Professor Luoxin Wang (Wuhan Textile University) for their critical comments on this manuscript. Finally, the authors thank the Computational Center of Baicheng Normal University.

References

1 L. Ke, W. Zhang and H. Qian, *Jiangsu. Food. Fermn*, 2001, **2**, 19–21.
2 H. Atsushi, N. Toru, O. Takae and T. Kiyohisa, *J. Neurochem.*, 1993, **60**, 783–786.
3 H. Wolosker, S. Blackshaw and S. H. Snyder, *Proc. Natl. Acad. Sci. U. S. A.*, 1999, **96**, 13409–13414.
4 G. Tsai, P. Yang, L.-C. Chung, N. Lange and J. T. Coyle, *Biol. Psychiatry*, 1998, **44**, 1081–1089.
5 N. Liang and A. Datta, *J. Org. Chem.*, 2005, **70**, 10182–10185.
6 S. A. Mitchell, B. D. Oates, H. Razavi and R. Polt, *J. Org. Chem.*, 1998, **63**, 8837–8842.
7 P. Bhaket, C. S. Stauffer and A. Datta, *J. Org. Chem.*, 2004, **69**, 8594–8601.
8 K. Hamase, A. Morikawa and K. Zaitsu, *J. Chromatogr. B: Anal. Technol. Biomed. Life Sci.*, 2002, **781**, 73–91.
9 N. Fujii, *Origins Life Evol. Biospheres*, 2002, **32**, 103–127.
10 H. D. Dakin, *Am. Chem. J.*, 1910, **44**, 48.
11 A. Neuberger, in *Advances in protein chemistry*, ed. M. L. Anson and J. T. Edsall, Academic Press, 1948, vol. 4, pp. 297–383.
12 E. J. Ebbers, G. J. A. Ariaans, J. P. M. Houbiers, A. Bruggink and B. Zwanenburg, *Tetrahedron*, 1997, **53**, 9417–9476.
13 G. G. Smith and T. Sivakua, *J. Org. Chem.*, 1983, **48**, 627–634.
14 R. Sullivan, M. Pyda, J. Pak, B. Wunderlich, J. R. Thompson, R. Pagni, H. Pan, C. Barnes, P. Schwerdtfeger and R. Compton, *J. Phys. Chem. A*, 2003, **107**, 6674–6680.
15 R. Liardon and R. F. Hurrell, *J. Agric. Food Chem.*, 1983, **31**, 432–437.
16 D. E. Schwass and J. W. Finley, *J. Agric. Food Chem.*, 1984, **32**, 1377–1382.
17 S. Blanco, M. E. Sanz, J. C. López and J. L. Alonso, *Proc. Natl. Acad. Sci. U. S. A.*, 2007, **104**, 20183–20188.
18 S. Jarmelo, L. Lapinski, M. J. Nowak, P. R. Carey and R. Fausto, *J. Phys. Chem. A*, 2005, **109**, 5689–5707.
19 B. Lambie, R. Ramaekers and G. Maes, *J. Phys. Chem. A*, 2004, **108**, 10426–10433.
20 K. He and W. D. Allen, *J. Chem. Theory Comput.*, 2016, **12**, 3571–3582.
21 D.-C. Sun, Z.-C. Wang, F. Gao, H.-Y. Yan, Y. Zhuang and X.-C. Yang, *J. Xiamen Univ., Nat. Sci.*, 2019, **58**, 471–478.
22 Z.-C. Wang, F. Gao, Y.-H. Zhao, H. Tong and Z.-M. Mei, *J. Zhejiang Univ., Sci.*, 2015, **42**, 189–197.
23 Z.-C. Wang, Y.-Q. Wang, H.-Y. Yan and H. Tong, *Acta Sci. Nat. Univ. Sunyatseni*, 2016, **55**, 57–65.
24 C. Tian, P. Xiu, Y. Meng, W. Zhao, Z. Wang and R. Zhou, *Chem. – Eur. J.*, 2012, **18**, 14305–14313.
25 F. Gao, X.-L. Wang, H. Tong, F. Liu, Z.-M. Mei and Z.-C. Wang, *J. Jilin Univ. Sci.*, 2016, **54**, 1161–1167.
26 L. L. de Zwart, J. H. N. Meerman, J. N. M. Commandeur and N. P. E. Vermeulen, *Free Radical Biol. Med.*, 1999, **26**, 202–226.
27 C. Lee, W. Yang and R. G. Parr, *Phys. Rev. B: Condens. Matter Mater. Phys.*, 1988, **37**, 785–789.
28 P. J. Stephens, F. J. Devlin, C. F. Chabalowski and M. J. Frisch, *J. Phys. Chem.*, 1994, **98**, 11623–11627.
29 M. Reiher, O. Salomon and B. Artur Hess, *Theor. Chem. Acc.*, 2001, **107**, 48–55.
30 A. D. Becke, *Phys. Rev. A: At., Mol., Opt. Phys.*, 1988, **38**, 3098–3100.
31 A. D. Becke, *J. Chem. Phys.*, 1993, **98**, 1372–1377.
32 A. D. Becke, *J. Chem. Phys.*, 1993, **98**, 5648–5652.
33 W. J. Hehre, R. Ditchfield and J. A. Pople, *J. Chem. Phys.*, 1972, **56**, 2257–2261.
34 T. Clark, J. Chandrasekhar, G. W. Spitznagel and P. V. Ragué Schleyer, *J. Comput. Chem.*, 1983, **4**, 294–301.
35 J. S. Binkley and J. A. Pople, *Int. J. Quantum Chem.*, 1975, **9**, 229–236.
36 C. Møller and M. S. Plesset, *Phys. Rev.*, 1934, **46**, 618–622.
37 M. J. Frisch, J. A. Pople and J. S. Binkley, *J. Chem. Phys.*, 1984, **80**, 3265–3269.

38 J. M. Anglada and J. Gonzalez, *ChemPhysChem*, 2009, **10**, 3034–3045.
39 Y. J. Hong and D. J. Tantillo, *Nat. Chem.*, 2009, **1**, 384.
40 Y. Luo, S. Maeda and K. Ohno, *Chem. Phys. Lett.*, 2009, **469**, 57–61.
41 M.-P. Gaigeot, A. Cimas, M. Seydou, J.-Y. Kim, S. Lee and J.-P. Schermann, *J. Am. Chem. Soc.*, 2010, **132**, 18067–18077.
42 J. Gonzalez and J. M. Anglada, *J. Phys. Chem. A*, 2010, **114**, 9151–9162.
43 P. Gutta and D. J. Tantillo, *J. Am. Chem. Soc.*, 2006, **128**, 6172–6179.
44 L.-C. Li, F. Hu, W.-F. Cai, A.-M. Tian and N.-B. Wong, *THEOCHEM*, 2009, **911**, 98–104.
45 X. Xu, R. P. Muller and W. A. Goddard, *Proc. Natl. Acad. Sci. U. S. A.*, 2002, **99**, 3376–3381.
46 A. V. Marenich, C. J. Cramer and D. G. Truhlar, *J. Phys. Chem. B*, 2009, **113**, 6378–6396.
47 M. J. Frisch, G. W. Trucks, H. B. Schlegel, G. E. Scuseria, M. A. Robb, J. R. Cheeseman, G. Scalmani, V. Barone, B. Mennucci, G. A. Petersson, H. Nakatsuji, M. Caricato, X. Li, H. P. Hratchian, A. F. Izmaylov, J. Bloino, G. Zheng, J. L. Sonnenberg, M. Hada, M. Ehara, K. Toyota, R. Fukuda, J. Hasegawa, M. Ishida, T. Nakajima, Y. Honda, O. Kitao, H. Nakai, T. Vreven, J. A. Montgomery, J. E. Peralta, F. Ogliaro, M. Bearpark, J. J. Heyd, E. Brothers, K. N. Kudin, V. N. Staroverov, R. Kobayashi, J. Normand, K. Raghavachari, A. Rendell, J. C. Burant, S. S. Iyengar, J. Tomasi, M. Cossi, N. Rega, J. M. Millam, M. Klene, J. E. Knox, J. B. Cross, V. Bakken, C. Adamo, J. Jaramillo, R. Gomperts, R. E. Stratmann, O. Yazyev, A. J. Austin, R. Cammi, C. Pomelli, J. W. Ochterski, R. L. Martin, K. Morokuma, V. G. Zakrzewski, G. A. Voth, P. Salvador, J. J. Dannenberg, S. Dapprich, A. D. Daniels, Ö. Farkas, J. B. Foresman, J. V. Ortiz, J. Cioslowski and D. J. Fox, *Gaussian 09, Revision B.01*, Gaussian, Inc., Wallingford, CT, 2009.
48 L. Gorb, Y. Podolyan and J. Leszczynski, *THEOCHEM*, 1999, **487**, 47–55.
49 L. Gorb and J. Leszczynski, *J. Am. Chem. Soc.*, 1998, **120**, 5024–5032.
50 Z. Cao, Y. Peng, T. Yan, S. Li, A. Li and G. A. Voth, *J. Am. Chem. Soc.*, 2010, **132**, 11395–11397.
51 C. Dellago, M. M. Naor and G. Hummer, *Phys. Rev. Lett.*, 2003, **91**, 139902.
52 N. Agmon, *Chem. Phys. Lett.*, 1995, **244**, 456–462.

